

LA-UR-16-22477

Approved for public release; distribution is unlimited.

Title: Evaluation of a self-equilibrium cutting strategy for the contour method of residual stress measurement

Author(s): Muransky, Ondrej  
Hamelin, Cory J  
Hosseinzadeh, F  
Prime, Michael Bruce

Issued: 2016-04-13 (Draft)

---

Muránsky O, Hamelin CJ, Hosseinzadeh F, Prime MB (2017), "Evaluation of a self-equilibrium cutting strategy for the contour method of residual stress measurement," *International Journal of Pressure Vessels and Piping*. DOI: 10.1016/j.ijpvp.2017.04.002

**Disclaimer:**

Los Alamos National Laboratory, an affirmative action/equal opportunity employer, is operated by the Los Alamos National Security, LLC for the National Nuclear Security Administration of the U.S. Department of Energy under contract DE-AC52-06NA25396. By approving this article, the publisher recognizes that the U.S. Government retains nonexclusive, royalty-free license to publish or reproduce the published form of this contribution, or to allow others to do so, for U.S. Government purposes. Los Alamos National Laboratory requests that the publisher identify this article as work performed under the auspices of the U.S. Department of Energy. Los Alamos National Laboratory strongly supports academic freedom and a researcher's right to publish; as an institution, however, the Laboratory does not endorse the viewpoint of a publication or guarantee its technical correctness.

# Evaluation of a self-equilibrium cutting strategy for the contour method of residual stress measurement

O. Muránsky<sup>1</sup>, C.J. Hamelin<sup>1</sup>, F. Hosseinzadeh<sup>2</sup>, M.B. Prime<sup>3</sup>

<sup>1</sup>ANSTO, Institute of Materials Engineering, Lucas Heights, NSW, Australia

<sup>2</sup>Open University, Materials Engineering, Milton Keynes, MK7 6BJ, UK

<sup>3</sup>Los Alamos National Laboratory, Los Alamos, NM 87545, USA

## Abstract

An assessment of cutting-induced plasticity (CIP) is performed, by finite element (FE) prediction of the plastic strain accumulation along the cut tip when the EDM wire sections the NeT TG4 weld benchmark specimen along two cutting directions. The first direction corresponds to a conventional (C) cutting strategy, whereby the EDM wire cuts through the thickness of the weld specimen and travels in a direction transverse to the weld. The second direction corresponds to a self-equilibrating cutting (SE) strategy, whereby the EDM wire cuts across the transverse direction of the weld specimens and travels through the thickness of the plate. The cutting thus progresses simultaneously through the compression-tension-compression regions of present weld residual stress (WRS) field. This type of cutting strategy is believed to minimize the CIP by minimising residual stress redistribution during cutting, due to stress equilibration across the sectioned material. The simulated cutting procedures are conducted under a range of clamping conditions to assess whether mechanical restraint has a primary or secondary influence on CIP accumulation. Both predictions of CIP and the resultant back-calculated WRS demonstrate that (i) mechanical restraint is the primary variable influencing CIP development, and (ii) under no circumstance does a self-equilibrating cutting strategy perform significantly better than a conventional cutting approach. The reason that self-equilibrating cuts are not effective is illustrated by calculating the Mode I ( $K_I$ ) stress intensity factor (SIF) along the cut tip, and correlating trends in  $K_I$  to CIP development.

*Keywords: Residual stress; contour method; optimisation; finite element analysis; cutting direction*

## 1. Introduction

The development of weld residual stresses (WRS) is known to have adverse effects on the structural integrity of welded components in service [1], leading to extensive research into the magnitude and distribution of WRS in engineering components. Several international round-robin studies [2-4] have been conducted in an effort to establish best-practice guidelines for the measurement and prediction of WRS in welded structures. In these studies, it has been recognised that diffraction-based techniques using neutron or synchrotron X-ray sources are of great benefit to the industry (e.g. EDF Energy and AREVA work closely with European Network on Neutron Techniques Standardisation for Structural Integrity, NeT). Neutron diffraction techniques can capture the full three-dimensional stress state of the material [5, 6], while synchrotron diffraction techniques can typically capture WRS in two dimensions (assuming plane-stress conditions exist) at a significantly higher sampling rate and spatial resolution [7]. However, both diffraction techniques are limited by the penetration depth of the source (beam attenuation), as well as cross-weld changes in microstructure and chemical composition, which necessitate the extraction of stress-free reference samples to account for variations in crystal lattice spacing<sup>1</sup> [5, 8, 9].

Unlike diffraction-based approaches to WRS measurement, stress-relief or relaxation techniques are destructive (i.e. the WRS field is altered in the measurement process and the measurement cannot be repeated) and are usually limited to capturing WRS in one or two directions [10-16]. However, these techniques can often measure much thicker engineering components [17-20] and are much less sensitive to any cross-weld microstructural or compositional variations [21]. In addition, the infrastructure required to measure WRS using stress-relief techniques is readily available relative to neutron and synchrotron sources, making them an attractive alternative in many circumstances.

One of the increasingly common stress-relief techniques is the contour method [10, 12, 22], which is based on Bueckner's principle of elastic superposition [23]. The contour method has been shown to be effective in measuring two-dimensional residual stress maps in engineering components [24-30]. The technique is performed in four stages: (i) the specimen is sectioned (cut) using electric discharge machining (EDM) along the plane-of-cut in the region of interest; (ii) the resultant out-of-plane deformation (OoPD) caused by internal stress relaxation is measured, using either optical ranging or a coordinate-measuring machine (CMM); (iii) the measured data is smoothed and fitted using numerical algorithms to reduce errors introduced by the cutting process<sup>2</sup>; and (iv) the original (i.e. pre-cut) internal stresses are then back-calculated using an elastic finite element (FE) analysis. In the final stage, the processed OoPD data is imposed as a geometric boundary condition onto an elastic FE model of the cut specimen. Assuming the fully elastic stress-relief of the original inter-

---

<sup>1</sup> Knowledge of the stress-free lattice spacing is essential for diffraction-based measurements to calculate elastic lattice strain, which can then be used in stress calculations.

<sup>2</sup> While data processing is often performed to reduce signal noise, it is also used to remove anti-symmetric component errors from the analysis, which are generated by shear stresses or crooked cutting.

nal stresses during specimen cutting, this methodology analytically recovers the original residual stress field in the direction perpendicular to the plane-of-cut.

Fully elastic recovery does not always occur during cutting, however. The high-magnitude WRS and stress intensification near the leading edge of the cut can lead to the accumulation of cutting-induced plasticity (CIP), which directly influences the measured OoPD along the plane-of-cut. This ultimately leads to errors in the back-calculation of WRS, which inherently assumes fully elastic stress-relief of internal stresses during the specimen sectioning [31-35]. In terms of establishing best-practise guidelines for the contour method, the effective minimisation of CIP is one of the most active areas of research pertaining to contour methodology. Recent work by Hosseinzadeh *et al.* [35] experimentally demonstrates how different cutting configurations can be employed to minimise the amount of CIP in the contour method. These cutting configurations examine: (i) the extent of mechanical clamping used during the cutting process; (ii) the number and location of pilot holes, used to invoke self-constraint within the weldment; and (iii) the number, direction and length of the cuts used to release WRS in an optimal fashion, thus minimising the amount of CIP and its effect on the contour method accuracy. Unfortunately, optimising a cutting configuration experimentally is a costly and time-consuming process.

An attractive alternative to experimental analysis for process optimisation lies in simulating the contour method cutting technique. The work of Muránsky *et al.* [15] presents a numerical cutting simulation validated using the experimental results of Hosseinzadeh *et al.* [35]. This work shows that not only can the level of CIP be captured using numerical analysis, but process optimisation can be carried out to eliminate the costly battery of tests that would otherwise be required. Hence, the present work uses numerical finite element (FE) simulations to examine the potential of self-equilibrating (SE) contour cutting strategy for measuring residual stresses. A self-equilibrating cutting strategy is of great interest to the contour measurement community as it is believed to be an encouraging new approach to minimise CIP and thus improve the accuracy of contour method. But is a such cutting strategy truly effective? In following section, the efficiency of self-equilibrating (SE) and conventional (C) cutting strategies in limiting the effects of CIP is discussed in detail.

## **2. NeT TG4 weld specimen**

The European Network on Neutron Techniques Standardisation for Structural Integrity (NeT) has formed a Task Group 4 (TG4) to establish best-practice guidelines for the measurement and prediction of WRS in multi-pass austenitic steel welds. A series of benchmark specimens have been produced under the auspices of NeT TG4 for the purposes of WRS measurement and FE weld model validation. The nominally identical specimens comprise a three-pass slot weld in AISI 316LN austenitic steel. Individual weld passes were deposited using a mechanised tungsten inert gas (TIG) welding process. The filler metal used was ER316L, which has a slightly different chemical composition relative to the 316LN parent

metal [2]. The nominal dimensions of the plate, shown in Fig. 1, are 150 (X) × 18 (Y) × 194 (Z) mm with an 80-mm long and 6-mm deep centreline slot aligned with the Z-direction.

An FE weld model was constructed for NeT TG4 using the ABAQUS commercial software package. Due to process symmetry, a half-model was used with the symmetry plane (Fig. 1, D plane) running parallel to the weld centreline. A sequentially-coupled numerical analysis was then employed to simulate the welding process, with the heat transfer solution from the thermal FE analysis serving as input for the mechanical FE analysis, where weld residual stresses (WRS) and welding-induced plasticity (WIP) are predicted [2]. Both thermal and mechanical models comprised 38,220 hexahedral quadratic elements; the thermal model used quadratic heat transfer elements (ABAQUS designation DC3D20) while mechanical analyses used reduced-integration quadratic stress elements (ABAQUS designation C3D20R). The weld modelling analysis employed the Lemaitre-Chaboche combined isotropic-kinematic hardening model [36] to accurately capture the welding-induced cyclic hardening of 316LN alloy during the welding process. Annealing was controlled via a two-stage annealing functionality developed for the ABAQUS package [37].

WRS predictions were compared against measurements obtained from the NeT TG4 benchmark specimens, using both neutron and synchrotron X-ray stress measurements in Ref. [2]. For the sake of brevity, Fig. 2 compares the predicted and synchrotron-measured longitudinal WRS on the plane of interest (Fig. 1, B plane). The predicted WRS distribution in the specimen – particularly along the intended plane-of-cut – is in good agreement with experimental results. Therefore, the numerical solution from this welding simulation can be used as input data for subsequent contour cutting simulations, and the analyst can be confident that this weld model contains representative WIP and WRS distributions.

### **3. Contour cutting FE simulations**

Figures 1 and 2 show schematically the self-equilibrating cutting strategy and the conventional cutting strategy. Conventionally, the EDM wire is oriented to minimize the thickness of material being cut because that generally improves the quality of the cut [10], and this quality is often key to getting the best possible OoPD measurements [38-41]. A detailed study on plasticity and the slitting method [42], which similarly involves EDM cutting into residual stress fields, shows that most plasticity occurs at the cut tip, which is caused by the cumulative effect of all stresses relieved by the cut up to that point. Plasticity studies on the slitting method [42], deep hole method [43], and the contour method [13, 31-34] support that conclusion. When a conventional single cut is employed on a stress distribution like the one found in the NeT TG4 weld specimen (Fig. 2), the cut initially relaxes stresses that are entirely compressive, causing a significant redistribution of compressive stresses to the cut tip that could exceed the yield strength of the material, leading to CIP. In contrast, if we consider starting the cutting process at the top of the specimen with the wire oriented along the sample X dimension, it can be seen (Fig. 2) that such a cut would release an approximately balanced or self-equilibrating stress distribution along the X direction (compression-

tension-compression regions of internal WRS field). It has been hypothesized that this sort of self-equilibrating cutting strategy would result in lower net stress redistribution to the cut tip, therefore reducing CIP [44]. Although the detailed residual stresses are not known prior to measurement, knowledge of processing conditions often allow one to identify the likely regions for tensile or compressive stresses and then choose the cutting orientation most likely for self-equilibrium.

In terms of contour method measurements, previous studies of the NeT TG4 specimen [2, 45] identified the longitudinal (Z) WRS profile to be the most significant. Therefore, cross-weld planar sectioning (plane B, Fig. 1) was simulated such that the resultant OoPD would capture the longitudinal WRS distribution. Similarly to the weld model, the contour method simulations have employed an isotropic-kinematic hardening model [2, 36], which allows the most accurate simulation of the constitutive material response [45]. A mechanical FE analysis is required to simulate the EDM cutting process; however, this analysis first requires the WRS and associated WIP fields from the validated weld simulation to be mapped onto the cutting model as the initial material state. The mapping process from the weld FE model [2] to cutting FE model was carried out over two stages:

- (i) The assumption of process symmetry used for welding simulation is no longer valid for the cutting processes investigated, so the half-model solution (WRS, WIP) from the welding simulation is mirrored about the symmetry plane (plane D, Fig.1) to allow mapping onto a full 3D contour cutting model [46].
- (ii) Welding-induced distortion was removed from the welding solution to allow direct mapping of the welded material condition onto the undistorted contour cutting model. These distortions have no significant effect on the initial WRS distribution in the specimen and can be neglected [46].

Because high stress gradients are expected along the plane-of-cut as the cut progresses, the FE mesh used for the cutting model was significantly refined near the region of the cut. Considering both the use of a full 3D model and significant mesh refinement, the number of elements used increased from 38,220 for the welding model to 451,368 for the cutting model. Reduced-integration hexahedral quadratic elements stress elements (C3D20R) were used in all cutting models.

In the conventional cutting strategy, the EDM wire is aligned in normal direction (Y), and travels in the transverse direction (X) until sectioning is complete. To simulate the conventional cutting strategy, 470 through-thickness element sets measuring  $0.32 (X) \times 18 (Y) \times 0.32 (Z)$  mm were defined as schematically shown Fig. 1. For the self-equilibrating cutting strategy, the EDM wire is aligned in the transverse direction (X), and it travels in the normal direction (Y) so that it cuts through compression-tension-compression regions of WRS distribution (Fig. 2). To simulate this cutting strategy, only 58 element sets measuring  $150 (X) \times 0.32 (Y) \times 0.32 (Z)$  mm were defined to cover the through-thickness cut. Contour cutting was then simulated by the incremental removal of these predefined element sets, representing

the progressive sectioning carried out by a 0.25-mm thick EDM wire<sup>3</sup>. Strain-rate effects are not considered in the analyses; the element sets were progressively removed over an arbitrarily chosen 1-s time interval, and rate-independent material properties were used. Once the cutting process has been completed, the OoPD in the longitudinal (Z) direction across each cut surface is recorded. The longitudinal WRS distribution is then back-calculated using an identical approach to that used for experimental contour measurement [12]: (i) a stress-free fully elastic FE model of the cut specimens with the flat cut surface was constructed; and (ii) the recorded longitudinal OoPD component was then applied as a displacement boundary condition on the cut surface, thus recovering the original longitudinal WRS field along the plane-of-cut (assuming that measured OoPD is fully elastic).

Both cutting strategies are examined under three different clamping configurations, with different prescribed boundary conditions representing variations in mechanical restraint during the cutting process. These configurations are schematically shown in Fig. 3. To simulate the clamping process, surface boundary conditions are prescribed whereby nodal displacements are fully constrained in all directions ( $U_1, U_2, U_3=0$ )<sup>4</sup>.

No-Clamps Configuration (Fig. 3a): Three pin-constraint boundary conditions are placed in the corners of the FE model to prevent rigid-body rotation upon cutting.

Far-Clamps Configuration (Fig. 3b): Two large (150 × 20) mm clamps are placed along the outer edges of the FE model, aligned with the specimen X axis and running along the entire edge of the specimen.

Close-Clamps Configuration (Fig. 3c): Two large (150 × 20) mm clamps are placed adjacent to the plane-of-cut, aligned with the specimen X axis and running along the entire edge of the specimen.

#### 4. Stress intensity factor (SIF) analyses

Fracture mechanics analyses were employed to help interpret the FE results and the hypothesis that self-equilibrating stresses will act together to reduce CIP. Previous studies of slitting and contour methods showed that cut tip plasticity correlates well to the stress intensity factor (SIF) at the cut tip [13, 42]. Even for a round-bottomed, e.g., blunt, EDM slot the SIF reveals the stress concentration at the cut tip caused by stress redistribution as the cut progresses and should scale the plasticity effects. The Mode I SIF ( $K_I$ ) at the cut tip was calculated to assess the potential for self-equilibrating cuts to reduce CIP relative to conventional cutting strategies. For the conventional cutting strategy, the longitudinal (Z) WRS shown in Fig. 2b were averaged over the plate thickness (Y) to give an average stress,  $\sigma_z(Y)$ , used to calculate  $K_I$  as a function of the cut length in the transverse (X) direction. For the

---

<sup>3</sup> The width of the simulated cut (0.32 mm) is greater than the EDM wire thickness (0.25 mm) to account for the excess material removed by EDM.

<sup>4</sup> Note, these boundary conditions are applied on both the top surface and on the bottom surface of the FE models and they represent an ideal rigid clamping, which is virtually impossible to achieve in practice. Hence, the obtained prediction may produce non-conservative results.

self-equilibrating cut, the first approximation was to average the longitudinal WRS over the transverse direction to give an average stress,  $\sigma_z(X)$ , used to calculate  $K_I$  as a function of cut length, which is now in the normal (Y) direction. Since the stresses nearly balance in the transverse (X) direction, this approximation corresponds to the hypothesis that self-equilibrating cutting will lead to reduced plasticity when the released stresses balance along the cut.

The alternate approximation for the self-equilibrating cut was to assume that the stresses act independently in the transverse (X) direction, meaning that there is no balancing effect. Stresses were taken along lines at  $X = 0$  and  $X = 68$  (Fig. 2b) to look at tensile and compressive stress regions, respectively, and used again to estimate  $K_I$  as a function of cut depth in the normal (Y) direction.  $K_I$  was numerically calculated from these one-dimensional stress profiles using a weight function approach [47-49]. This calculation also does not include crack closure, which is consistent with the cutting simulations; therefore, negative values of  $K_I$  are permissible. Estimating  $K_I$  this alternate way assumes that the specimen is unconstrained during cutting process, which is simpler to interpret and more illustrative of the effects of the cutting direction. Therefore, the predicted  $K_I$  profiles are compared with the results of the unconstrained cutting simulation (Fig. 3a) rather than the cutting configurations employing mechanical constraint (Fig. 3b,c).

## 5. Results and Discussion

### 5.1 Contour cutting FE simulations

Figure 4 presents the predicted, depth-resolved OoPD profiles across the plane-of-cut for conventional and self-equilibrating cutting strategies under the three different clamping configurations. The OoPD profiles can be directly compared against an elastic OoPD benchmark profile (black) obtained by simulating the contour cutting process using a fully elastic FE model (i.e. plasticity was allowed during the sectioning, thus all clamping strategy lead to the same result). This fully elastic OoPD profile thus represents an ideal measurement data without any CIP contribution. Note that using the ideal OoPD profile in the back-calculated stress analysis would lead to the recovery of the exact original (pre-cut) WRS. Several observations can be made from the comparison of the elasto-plastic predictions of longitudinal OoPD:

- (i) The OoPD profiles differ considerably from the ideal fully elastic profile when employing “no-clamps” (Fig. 3a) and “far-clamps” (Fig. 3b) configurations. This implies a large contribution of CIP to the predicted OoPD. These contributions appear considerably reduced when using the “close-clamps” configuration (Fig. 3c), regardless of the cutting strategy (i.e. conventional or self-equilibrating). This trend confirms that significant mechanical restraint close to the plane-of-cut effectively prevents WRS redistribution during the cutting process, which then leads to a reduction in CIP.

- (ii) Deviations in predicted OoPD from an ideal elastic solution can be observed for conventional cutting strategies in Figs. 4a-c. For the “no-clamps” configuration, this deviation (and thus, CIP) occurs along the first half of the cut. For the “far-clamps” configuration, the deviation occurs along the second half of the cut. This change in recorded OoPD clearly suggests that the presence of clamping will affect WRS redistribution, even when they are placed away from the plane-of-cut. Deviations when using the “close-clamps” configuration are minimal.
- (iii) Deviations in predicted OoPD from an ideal elastic solution can be observed for self-equilibrating cutting strategies in Fig. 4d-f. Unlike the results of the conventional cutting strategies, the initial OoPD profile along the first half of the self-equilibrating cut (i.e. near the top surface of the sample) agrees with the fully elastic idealisation, relative to the OoPD profile along the second half of the cut (i.e. near the bottom half of the surface). This trend suggests that CIP will consistently accumulate as self-equilibrating cuts progress, regardless of the clamping configuration used. Such a result is interesting as it agrees with the results of Kim et al. [44], in that the level of CIP is negligible near the start of the cut; however, Kim et al. do not consider the effects of CIP away from the surface where the cut starts[50], which renders their conclusions inapplicable to the contour method.
- (iv) Good agreement between elastic and elasto-plastic results is observed at all self-equilibrating cut depths near the region where  $X = \pm 37.5$  mm. These locations correspond to the regions where negligible levels of WRS are present in the sample (Fig. 2); therefore, it is clear that no significant stress redistribution occurs within these regions that lead to CIP.

In order to get a deeper understanding of the evolution of CIP<sup>5</sup> for the conventional and self-equilibrating contour cutting strategies, it is helpful to examine directly the level of CIP across the plane-of-cut as presented as percent strain in Fig. 5. To quantify the level of CIP for each cutting strategy and clamping configuration, the total magnitude (M) of CIP was calculated as the sum of absolute values of all CIP values across the plane-of-cut (B plane, shown in Fig. 5):

$$M(\text{CIP})_{\text{SE/C}} = \sum_{i=1}^n |\text{CIP}_i|, \quad (1)$$

where  $n$  is the number of nodes on the plane-of-cut in the given FE model, and  $\text{CIP}_i$  the cutting-induced plasticity value at a given nodal position. The most surprising observation from this assessment is that when using the “no-clamp” configuration (Fig. 5a) with the conventional cutting strategy, the overall magnitude (M) of accumulated CIP across the plane-of-cut is lower than when using the same cutting strategy with the “far-clamps” configuration (Fig. 5b). This result suggests that in some cases it might be better to avoid using any mechanical constraint of the specimen during the contour cutting process rather than using an

---

<sup>5</sup> In the present work, CIP is calculated by subtracting the longitudinal component of WIP (shown in Fig. 5) from the total plastic strain component in the longitudinal direction after cutting.

insufficient or improper clamping configuration. When the OoPD results (Fig. 4) are considered alongside the CIP results, it is evident that an unrestrained cutting process leads to CIP in the first half of the cut that leads to an inaccurate OoPD profile in this region (Fig. 4a). However, the compressive plasticity that occurs (Fig. 5a) leads to the relaxation of tensile stresses in the weld region that prevents CIP from occurring here. In contrast, placing clamps away from the weld (Fig. 3b) prevents CIP in the first half of the cut. The restraint is beneficial for the captured OoPD in this region (Fig. 4b), but it prevents the relaxation of the tensile WRS in the weld region that leads to significant CIP when this region is sectioned, causing a severe deviation of OoPD in the second half of the cut.

The CIP distributions in Fig. 5 also show that a self-equilibrating (SE) cutting strategy with a “no-clamps” configuration generates significantly more CIP relative to a conventional (C) cutting arrangement ( $M(CIP)_{SE} = 2505.8$ ;  $M(CIP)_C = 1685.7$ ). For clamped configurations however, the self-equilibrating cuts perform slightly better than conventional strategies – although the difference in terms of  $M(CIP)$  values is negligible. But from these results it is apparent that self-equilibrating cuts do not perform as well as conventional cuts in un-clamped configurations.

While the overall magnitude of CIP does not change significantly between conventional and self-equilibrating cuts under clamping configuration, there is significant difference in the location of CIP. To better understand what effect this difference in CIP location has, the back-calculated WRS taken from the predicted OoPD profiles in Fig. 3 are presented in Fig. 6. The level of accuracy of each method has been calculated using a root-mean-square (RMS) error, shown in Fig. 6, as follows:

$$\text{RMS Error} = \sqrt{\frac{1}{n} \sum_{i=1}^n (|WRS_{i,pc}| - |WRS_{i,bc}|)^2}, \quad (2)$$

where:  $WRS_{i,pc}$  represents the original (pre-cut) WRS in a given nodal position; and  $WRS_{i,bc}$  represents the back-calculated WRS in the corresponding nodal position  $i$ . It is clear that this RMS error directly correlates with the total magnitude of CIP shown in Fig. 5, and that sufficient clamping close to the weld best captures WRS in the present specimen regardless of cutting strategy. However, different cutting strategies possessing similar RMS errors do not possess similar back-calculated WRS distributions. Self-equilibrating cuts retain the symmetry observed in the original WRS field, while conventional cutting strategies demonstrate an asymmetry in the final distribution. This distinction is important since it would be clearer to the analyst whether or not CIP exists in a cut by examining the level of asymmetry in the final WRS profile (assuming a symmetric weld profile is expected). One would be unable to discern the level of CIP when a self-equilibrating cut is used, since WRS symmetry is maintained even though CIP is accumulated.

Regardless of clamping configuration, the results indicate a self-equilibrating cutting strategy poses little to no advantage relative to a conventional cutting strategy for the current NeT TG4 benchmark specimen. Such a result contradicts the earlier hypothesis that self-equilibrating cuts should perform better than conventional cuts since their equilibrating nature will restrict WRS redistribution. To better examine why this does not occur, the SIF analyses are examined.

#### 4.2 Stress intensity factor calculations

Figure 7 compares the Mode I SIF ( $K_I$ ) estimates with CIP predictions from the contour cutting FE simulation, assuming a “no-clamps” configuration (Fig. 3a). Line profiles of both the  $K_I$  distribution and the CIP predictions (Fig. 5a) are plotted versus non-dimensional cut lengths. Note that a SIF weight function for plate geometries was used in the  $K_I$  calculations. This function is valid until the cut length reaches 85% of the plate thickness, thus results are not plotted beyond that length. For conventional cutting strategies, the through-thickness averaging of longitudinal WRS,  $\sigma_z(Y)$ , seems to be a reasonable approximation for estimating  $K_I$  since there is a clear proportionality between CIP (taken at mid-depth,  $Y = 9$  mm) and  $K_I$ .

For a self-equilibrating cut, the  $K_I$  approximation that uses the average WRS in the transverse direction,  $\sigma_z(X)$ , shows negligible magnitudes and does not agree with trends in CIP taken either along the sample mid-width ( $X = 0$  mm) where large tensile stresses occur, or along the outer transverse edge ( $X = 68$  mm) where large compressive stresses occur. When the  $K_I$  approximation uses the local stresses at  $X = 0$  mm and  $X = 68$  mm, good agreement can be observed in the trends obtained relative to CIP trends in those locations, to a cut depth of over 20%. This result is a compelling indication that *the internal WRS act independently during the initial stages of cutting, rather than equilibrating to reduce stress redistribution and thus minimize the amount of CIP*. Note that if the WRS would have equilibrated along the length of the cut, calculated  $K_I$  in the given locations ( $X = 0$  mm,  $X = 68$  mm) would be higher than actual CIP predictions. Similar independent action of the WRS along the cut has been observed in other situations, such as cut closure in regions of compressive stress along a cut [51]. However, once the cut has progressed over 20% into the weld specimen, a sufficient amount of material has been freed to allow long-range equilibration of WRS. This equilibration manifests itself as a reduction in the CIP trends at each location in Fig. 7, relative to the corresponding  $K_I$  trends. However, while equilibration of the WRS across the plane of cut does exist, it is not sufficient to reduce the overall stress intensity, leading to continued CIP development as the cut progresses. It must be noted that such a result is only valid for the NeT TG4 stress distribution; improved results may be observed if the range over which self-equilibration occurs is relatively narrow, as may be expected for laser hybrid or electron beam welds. Further examination of the effects of stress distribution on the efficacy of self-equilibrating contour approaches is warranted.

## 6. Conclusions

A numerical approach to investigate the efficacy of self-equilibrating cutting strategies for optimal measurement of WRS via the contour has been conducted. Conventional and self-equilibrating cutting strategies employing three different clamping configurations were simulated in the present work. Both WRS and WIP distributions from a validated FE weld model was used as input and reference data for subsequent cutting simulations. The primary variables in these studies were the direction of cutting, and the size and location of mechanical restraints. It was concluded that the level of material restraint near the plane-of-cut had the largest impact on the accumulation of cutting-induced plasticity (CIP). Clamp locations away from the plane-of-cut permit extensive WRS redistribution, leading to stress localisation and significant CIP. Clamp locations near the plane-of-cut are only locally effective; thus for accurate results, clamping must be applied over the full transverse section of the sample.

Regarding cutting direction, conventional (C) cutting strategies perform better than self-equilibrating (SE) strategies when no clamping is present. Both cutting strategies perform equally well under two studied clamping conditions, which confirms the level of restraint applied is the primary factor affecting CIP development for the contour method. The reason that self-equilibrating cuts are ineffective at preventing CIP to any great extent is demonstrated using SIF analyses. These analyses show that in the early stages of self-equilibrating cutting, long-range internal stresses (WRS) do not readily equilibrate so the local stresses directly contribute to the local development of CIP along the plane-of-cut. An equilibrating effect of internal stresses across the plane-of-cut is observed as the cut progresses further into the sample; however, it is not sufficient to prevent further CIP. This effect may be more significant when the equilibrating residual stresses occupy a narrower region in the sample. Further examination of this relationship is warranted.

Considering these results, it is more beneficial to focus efforts instead on the use of advanced transverse sectioning techniques for welds. These techniques are amenable to the use of pilot holes and self-constraint that will ultimately eliminate the need for significant external clamping [35, 46]. Both numerical and experimental assessments of these techniques are currently underway to identify the optimal cutting procedure required for effective application of the contour method in welded structures.

## **Acknowledgements**

Residual stress measurements and welding simulations produced under the auspices of the NeT programme via Task Group 4 have significantly advanced best-practice guidelines for treatment of WRS and post-weld plastic strain, adding considerable value to the present work. Valuable discussions with Prof. John Bouchard regarding self-equilibrating cutting strategies for the contour method are also gratefully acknowledged. Part of this work was performed at Los Alamos National Laboratory, which is operated by the Los Alamos National Security, LLC for the National Nuclear Security Administration of the U.S. Department of Energy under contract DE-AC52-06NA25396.

## References

- [1] P.J. Withers. Residual stress and its role in failure Reports on Progress in Physics 70 (2007) 2211-2264.
- [2] O. Muránsky, M.C. Smith, P.J. Bendeich, T.M. Holden, V. Luzin, R.V. Martins, L. Edwards. Comprehensive numerical analysis of a three-pass bead-in-slot weld and its critical validation using neutron and synchrotron diffraction residual stress measurements, International Journal of Solids and Structures 49 (2012) 1045-1062.
- [3] P.J. Bouchard. The NeT bead-on-plate benchmark for weld residual stress simulation, International Journal of Pressure Vessels and Piping 86 (2009) 31-42.
- [4] M.C. Smith, A.C. Smith. NeT bead-on-plate round robin: Comparison of residual stress predictions and measurements, International Journal of Pressure Vessels and Piping 86 (2009) 79-95.
- [5] M.T. Hutchings, P.J. Withers, T.M. Holden, T. Lorentzen. Introduction to the Characterization of Residual Stress by Neutron Diffraction, CRC Press, 2005.
- [6] T.M. Holden. Neutron Diffraction. in: Schajer GS, (Ed.). Practical Residual Stress Measurement Methods. John Wiley & Sons, Ltd, 2013. pp. 195-223.
- [7] R.V. Martins, C. Ohms, K. Decroos. Full 3D spatially resolved mapping of residual strain in a 316L austenitic stainless steel weld specimen, Materials Science and Engineering: A 527 (2010) 4779-4787.
- [8] T.M. Holden, H. Suzuki, D.G. Carr, M.I. Ripley, B. Clausen. Stress measurements in welds: Problem areas, Materials Science and Engineering A 437 (2006) 33-37.
- [9] J. Rolph, N. Iqbal, M. Hoffman, A. Evans, M. Hardy, M. Glavicic, M. Preuss. The effect of d0 reference value on a neutron diffraction study of residual stress in a  $\gamma/\gamma'$  nickel-base superalloy, Journal of Strain Analysis for Engineering Design 48 (2013) 219-228.
- [10] M.B. Prime, A.T. DeWald. The Contour Method. in: Schajer GS, (Ed.). Practical Residual Stress Measurement Methods. John Wiley & Sons, Ltd., Chichester, WestSussex, UK, 2013.
- [11] G.S. Schajer, P.S. Whitehead. Hole Drilling and Ring Coring. in: Schajer GS, (Ed.). Practical Residual Stress Measurement Methods. John Wiley & Sons, Ltd, 2013. pp. 29-64.
- [12] M.B. Prime. Cross-Sectional Mapping of Residual Stresses by Measuring the Surface Contour after a Cut, Journal of Engineering Materials and Technology (2001) 162-168.
- [13] Y. Traore, P.J. Bouchard, J.A. Francis, F. Hosseinzadeh. A Novel Cutting Strategy for Reducing Plasticity Induced Errors in Residual Stress Measurements Made with the Contour Method. Pressure Vessels and Piping Division Conference, vol. PVP2011-57509. Baltimore, Maryland: Proceedings of the ASME, 2011.
- [14] P. Pagliaro, M.B. Prime, H. Swenson, B. Zuccarello. Measuring Multiple Residual-Stress Components using the Contour Method and Multiple Cuts, Experimental Mechanics 50 (2010) 187-194.
- [15] O. Muránsky, C.J. Hamelin, F. Hosseinzadeh, M.B. Prime. Mitigating Cutting-Induced Plasticity in the Contour Method, Part 2: Numerical Analysis, International Journal of Solids and Structures (2016).
- [16] M.R. Hill. The Slitting Method. in: Schajer GS, (Ed.). Practical Residual Stress Measurement Methods. John Wiley & Sons, Ltd, 2013. pp. 89-108.
- [17] W. Woo, G.B. An, V.T. Em, A.T. De Wald, M.R. Hill. Through-thickness distributions of residual stresses in an 80 mm thick weld using neutron diffraction and contour method, J Mater Sci 50 (2015) 784-793.
- [18] D.J. Smith. Deep Hole Drilling. in: Schajer GS, (Ed.). Practical Residual Stress Measurement Methods. John Wiley & Sons, Ltd, 2013. pp. 65-87.

- [19]R. Kaiser, M. Stefenelli, T. Hatzenbichler, T. Antretter, M. Hofmann, J. Keckes, B. Buchmayr. Experimental characterization and modelling of triaxial residual stresses in straightened railway rails, *The Journal of Strain Analysis for Engineering Design* 50 (2015) 190-198.
- [20]D.J. Smith, P.J. Bouchard, D. George. Measurement and prediction of residual stresses in thick-section steel welds, *Journal of Strain Analysis for Engineering Design* 35 (2000) 287-305.
- [21]W. Woo, H. Choo, M.B. Prime, Z. Feng, B. Clausen. Microstructure, texture and residual stress in a friction-stir-processed AZ31B magnesium alloy, *Acta materialia* 56 (2008) 1701-1711.
- [22]M.B. Prime. Measuring residual stress and the resulting stress intensity factor in compact tension specimens, *Fatigue and Fracture of Engineering Materials and Structures* 22 (1999) 195-204.
- [23]H.F. Bueckner. Field Singularities and Related Integral Representations, *Mechanics of Fracture* G.C. Sih, ed. (1973) 239-314.
- [24]B. Vrancken, V. Cain, R. Knutsen, J. Van Humbeeck. Residual stress via the contour method in compact tension specimens produced via selective laser melting, *Scripta Materialia* 87 (2014) 29-32.
- [25]P. Xie, H. Zhao, B. Wu, S. Gong. Evaluation of Residual Stresses Relaxation by Post Weld Heat Treatment Using Contour Method and X-ray Diffraction Method, *Experimental Mechanics* 55 (2015) 1329-1337.
- [26]Z. Zhang, Y. Yang, L. Li, B. Chen, H. Tian. Assessment of residual stress of 7050-T7452 aluminum alloy forging using the contour method, *Materials Science and Engineering: A* 644 (2015) 61-68.
- [27]P. Carlone, G.S. Palazzo. Characterization of TIG and FSW weldings in cast ZE41A magnesium alloy, *Journal of Materials Processing Technology* 215 (2015) 87-94.
- [28]M.R. Hill, M.D. Olson. Repeatability of the Contour Method for Residual Stress Measurement, *Experimental Mechanics* 54 (2014) 1269-1277.
- [29]M. Paquin, D. Thibault, P. Bocher, J.-B. Lévesque, Y. Verreman, K. Shinozaki. Assessment of cold cracking tests for low transformation temperature martensitic stainless steel multipass welds, *Weld World* 59 (2015) 521-532.
- [30]M.E. Kartal, Y.H. Kang, A.M. Korsunsky, A.C.F. Cocks, J.P. Bouchard. The influence of welding procedure and plate geometry on residual stresses in thick components, *International Journal of Solids and Structures* 80 (2016) 420-429.
- [31]S.H. Shin. FEM analysis of plasticity-induced error on measurement of welding residual stress by the contour method, *Journal of Mechanical Science and Technology* 19 (2005) 1885-1890.
- [32]R.J. Dennis, D.P. Bray, N.A. Leggatt, M. Turski. Assessment of the influence of plasticity and constraint on measured residual stresses using the contour method. *ASME Pressure Vessels and Piping Division Conference*, vol. Volume 6: Materials and Fabrication, Parts A and B. Chicago, IL, USA: ASME, 2008. p.477-485.
- [33]A.H. Mahmoudi, A.R. Hosseinzadeh, M. Jooya. Plasticity effect on residual stresses measurement using contour method, *International Journal of Engineering-Transactions A: Basics* 26 (2013) 1203-1212.
- [34]Y. Traoré, F. Hosseinzadeh, P.J. Bouchard. Plasticity in the Contour Method of Residual Stress Measurement, *Advanced Materials Research* 996 (2014) 337-342.

- [35]F. Hosseinzadeh, Y. Traore, P.J. Bouchard, O. Muránsky. Mitigating Cutting-Induced Plasticity in the Contour Method, Part 1: Experimental, International Journal of Solids and Structures submitted to the journal (2016).
- [36]J. Lemaitre, J.-L. Chaboche. Mechanics of Solid Materials, Cambridge University Press, 1994.
- [37]ABAQUS. A Novel Approach to Annealing using ABAQUS - behaviour with soft annealing. SIMULIA, 2007. p.A Novel Approach to Annealing using ABAQUS - behaviour with soft annealing.
- [38]F. Hosseinzadeh, J. Kowal, P.J. Bouchard. Towards good practice guidelines for the contour method of residual stress measurement. The Journal of Engineering: Institution of Engineering and Technology, 2014.
- [39]F. Hosseinzadeh, P. Ledgard, P. Bouchard. Controlling the Cut in Contour Residual Stress Measurements of Electron Beam Welded Ti-6Al-4V Alloy Plates, Experimental Mechanics 53 (2013) 829-839.
- [40]B. Ahmad, M. Fitzpatrick. Minimization and Mitigation of Wire EDM Cutting Errors in the Application of the Contour Method of Residual Stress Measurement, Metallurgical and Materials Transactions A (2015) 1-13.
- [41]M.B. Prime, A.L. Kastengren. The Contour Method Cutting Assumption: Error Minimization and Correction. in: Proulx T, (Ed.). Experimental and Applied Mechanics, Volume 6, vol. 17. Springer New York, 2011. pp. 233-250. Currently available at <http://www.lanl.gov/contour/>.
- [42]M.B. Prime. Plasticity effects in incremental slitting measurement of residual stresses, Engineering Fracture Mechanics 77 (2010) 1552-1566.
- [43]A.H. Mahmoudi, C.E. Truman, D.J. Smith, M.J. Pavier. The effect of plasticity on the ability of the deep hole drilling technique to measure axisymmetric residual stress, International Journal of Mechanical Sciences 53 (2011) 978-988.
- [44]H.K. Kim, H.E. Coules, M.J. Pavier, A. Shterenlikht. Measurement of Highly Non-Uniform Residual Stress Fields with Reduced Plastic Error, Experimental Mechanics 55 (2015) 1211-1224.
- [45]O. Muránsky, C.J. Hamelin, M.C. Smith, P.J. Bendeich, L. Edwards. The effect of plasticity theory on predicted residual stress fields in numerical weld analyses, Computational Materials Science 54 (2012) 125-134.
- [46]O. Muránsky, C.J. Hamelin, F. Hosseinzadeh, M.B. Prime. Mitigating Cutting-Induced Plasticity in the Contour Method, Part 2: Numerical Analysis, International Journal of Solids and Structures submitted to the journal (2016).
- [47]H.F. Bueckner. Novel principle for the computation of stress intensity factors, Zeitschrift fuer Angewandte Mathematik & Mechanik 50 (1970) 529-546.
- [48]T. Fett, D. Munz. Stress Intensity Factors and Weight Functions, Computational Mechanics, Inc., Billerica, MA, USA, 1997.
- [49]H. Tada, P.C. Paris, G.R. Irwin. The stress analysis of cracks handbook 3rd ed, The American Society of Mechanical Engineers, New York, NY, 2000.
- [50]H.K. Kim, private communication, 2015.
- [51]M.B. Prime, A.T. DeWald, M.R. Hill, B. Clausen, M. Tran. Forensic Determination of Residual Stresses and KI from Fracture Surface Mismatch, Engineering Fracture Mechanics 116 (2014) 158-171.



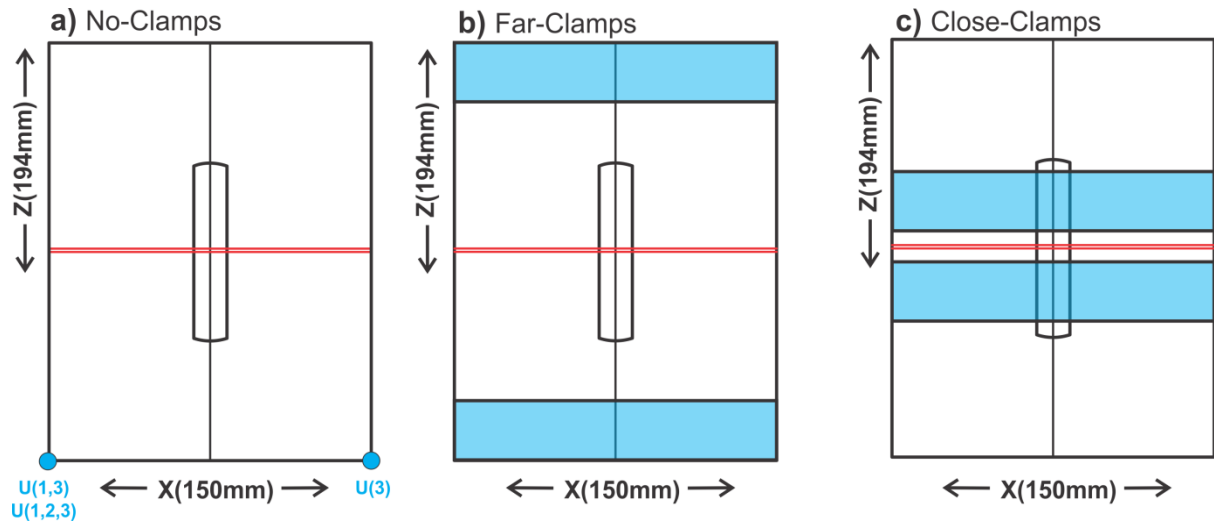


**Fig. 3:** Clamping configurations used to assess the importance of mechanical restraint: (a) "no clamps" configuration; (b) "far clamps" configuration; and (c) "close-clamps" configuration. Regions in blue denote clamped surfaces on the top and bottom of the plate specimen.

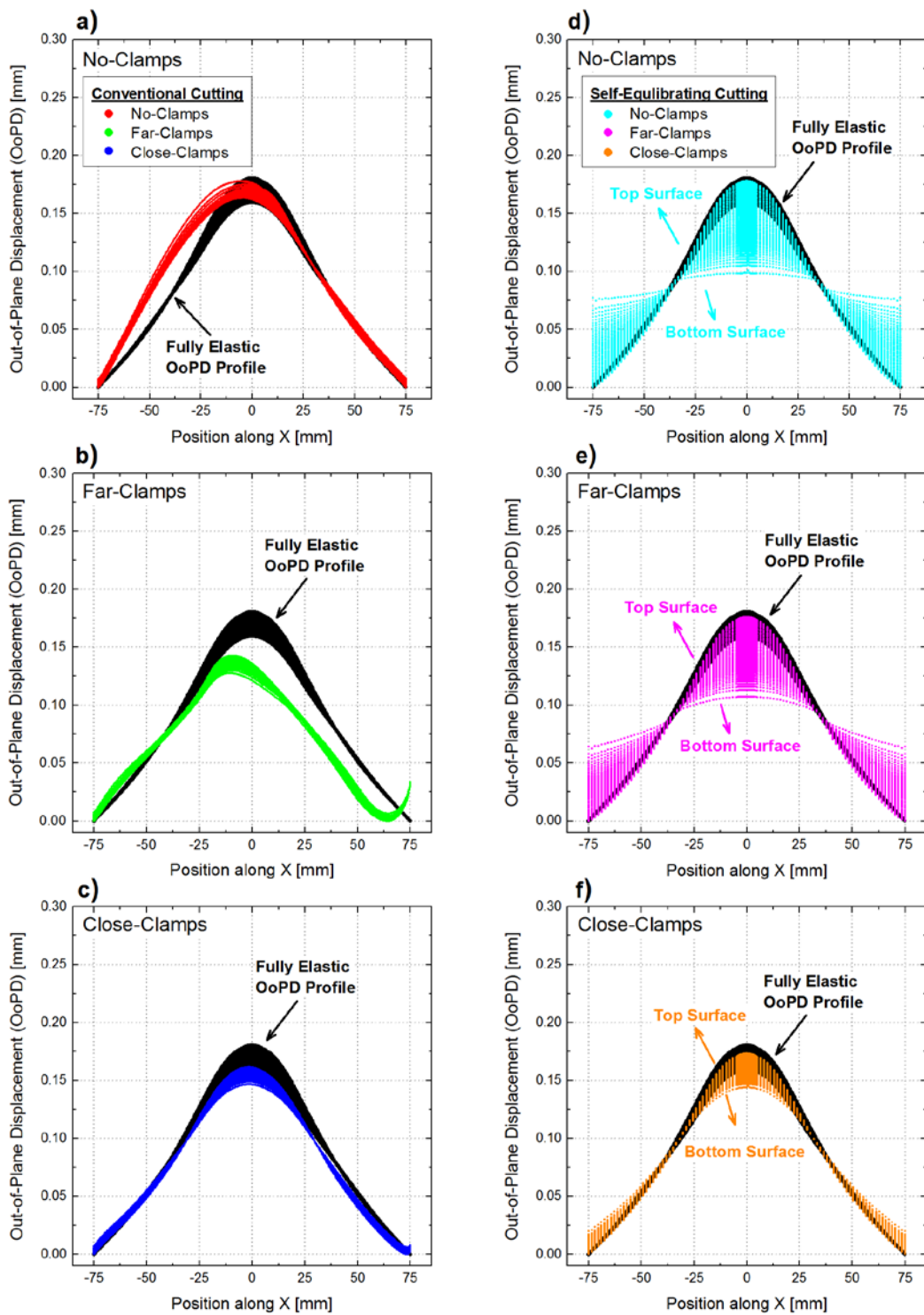


**Fig. 4:** Predicted out-of-plane displacement (OoPD) for conventional (a-c) and self-equilibrating (d-e) cutting strategies, under the clamping configurations shown in Fig. 3, compared to the fully elastic (ideal) OoPD profile (black).

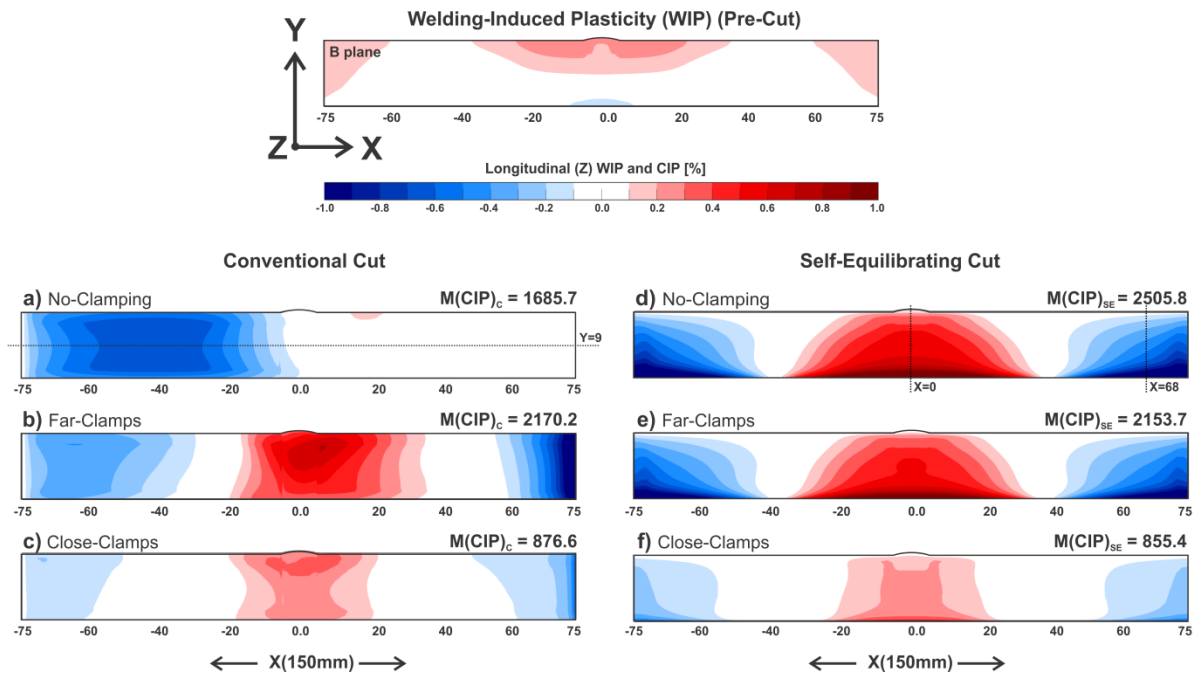


**Fig. 5:** (top) Predicted longitudinal (Z) welding-induced plasticity (WIP) [% strain] (post-welding, pre-cut). (a-f) Predicted longitudinal (Z) cutting-induced plasticity (CIP) [% strain], when using conventional (a-c) and self-equilibrating (d-f) contour cutting strategies under the clamping configurations shown in Fig. 3. Note that CIP is calculated by subtracting WIP from the total post-cut longitudinal (Z) plastic strain component.

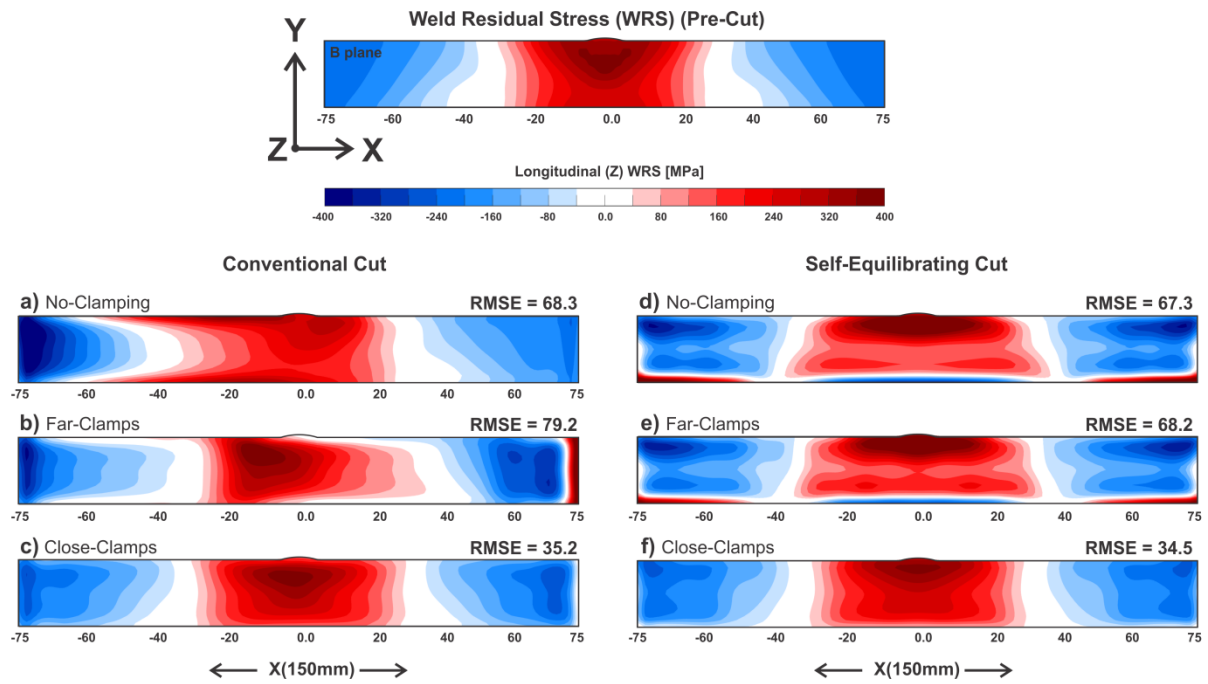


**Fig. 6:** (top) Predicted longitudinal (Z) weld residual stress (WRS) (post-welding, pre-cut). (a-f) The longitudinal (Z) WRS, back-calculated using the predicted OoPD data shown in Fig. 4. (a-c) Conventional cutting strategy; (d-f) self-equilibrating cutting strategy (see Fig. 1 and Fig. 2).

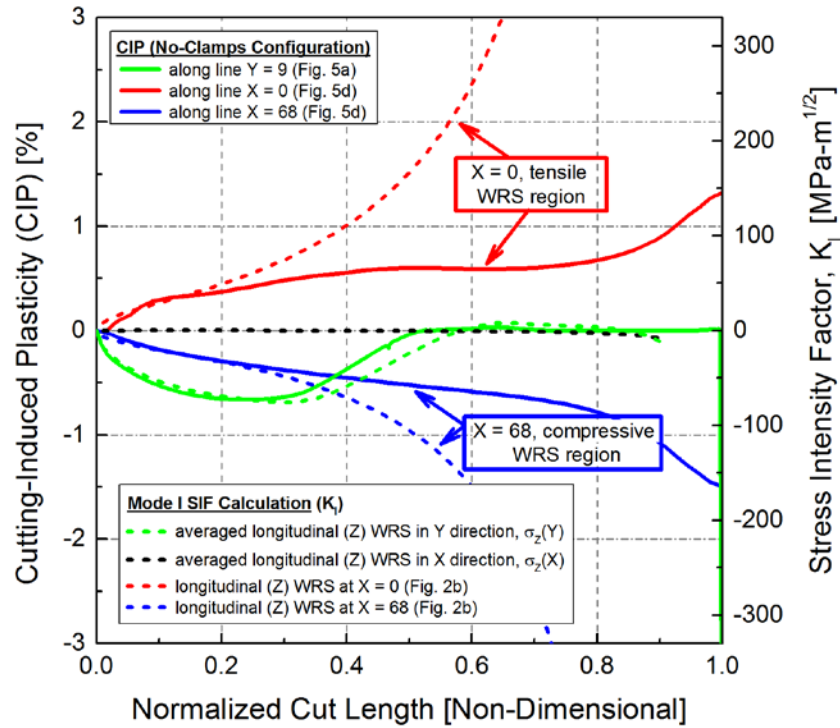


**Fig. 7:** Trends in cutting-induced plasticity (CIP) [% strain] development at the tip of the cut as it progresses, compared against the Mode I stress intensity factor,  $K_I$ . Conventional (green) and self-equilibrating (blue, red, black) cuts are examined. For the self-equilibrating cut,  $K_I$  trends are established in two ways: by calculating the net longitudinal stress along the transverse direction (black); and by direct application of local stresses at the weld centreline (red) and near the outer edge (blue) of the plate.